Incorporation of the δ-subunit into the epithelial sodium channel (ENaC) generates protease-resistant ENaCs in *Xenopus laevis*

Received for publication, February 20, 2018, and in revised form, March 14, 2018 Published, Papers in Press, March 25, 2018, DOI 10.1074/jbc.RA118.002543

Lukas Wichmann[‡§], **Kirsty Sophia Vowinkel**[§1], **Alexander Perniss**[§2], **Ivan Manzini**[§], **and Mike Althaus**[‡3]

From the [‡]*School of Natural and Environmental Sciences, Newcastle University, Ridley Building 2, Newcastle upon Tyne NE1 7RU, United Kingdom and the* [§]*Institute of Animal Physiology, Department of Animal Physiology and Molecular Biomedicine, Justus-Liebig University, 35392 Giessen, Germany*

Edited by Mike Shipston

The epithelial sodium channel (ENaC) is a critical regulator of vertebrate electrolyte homeostasis. ENaC is the only constitutively open ion channel in the degenerin/ENaC protein family, and its expression, membrane abundance, and open probability therefore are tightly controlled. The canonical ENaC is composed of three subunits (α, β, and γ), but a fourth δ-subunit may replace α and form atypical δβγ-ENaCs. Using *Xenopus laevis* as a model, here we found that mRNAs of the α- and δ-subunits are differentially expressed in different tissues and that δ-ENaC predominantly is present in the urogenital tract. Using whole-cell and single-channel electrophysiology of oocytes expressing *Xenopus* αβγ- or δβγ-ENaC, we demonstrate that the presence of the δ-subunit enhances the amount of current generated by ENaC due to an increased open probability, but also changes current into a transient form. Activity of canonical ENaCs is critically dependent on proteolytic processing of the α- and γ-subunits, and immunoblotting with epitope-tagged ENaC subunits indicated that, unlike α-ENaC, the δ-subunit does not undergo proteolytic maturation by the endogenous protease furin. Furthermore, currents generated by δβγ-ENaC were insensitive to activation by extracellular chymotrypsin, and presence of the δ-subunit prevented cleavage of γ-ENaC at the cell surface. Our findings suggest that subunit composition constitutes an additional level of ENaC regulation, and we propose that the *Xenopus* δ-ENaC subunit represents a functional example that demonstrates the importance of proteolytic maturation during ENaC evolution.

Mechanisms allowing salt and water conservation are some of the most important adaptations to a terrestrial environment and key in tetrapod evolution (1). The renin-angiotensin-aldosterone system evolved during water–land transition and is the major regulatory mechanism controlling the ionic composition of the extracellular milieu in vertebrates (1). A key target for the renin-angiotensin-aldosterone system is the epithelial sodium channel (ENaC)[4] in the apical membrane of principal epithelial cells in the aldosterone-sensitive distal nephron (2). ENaC represents the rate-limiting step for apical uptake of sodium ions and, in concert with the basolateral Na^+/K^+-ATPase, transepithelial sodium and, consequently, water absorption.

ENaC is the only member of the degenerin (DEG)/ENaC superfamily of proteins, which is constitutively open (2) and is therefore one of the most stringently regulated ion channels in vertebrates. Hormones, such as aldosterone and glucocorticoids, control ENaC expression (3), whereas a complex network of intracellular kinases regulates its membrane abundance (4). ENaC open probability (P_o) is modulated by intramembrane lipids (2) and is sensitive to changes in the extracellular environment (2), including the concentration of sodium ions (5), pH (6), or mechanical stimuli (7). In addition to these regulatory mechanisms, ENaC activity is linked to its maturation state through proteolytic processing of its subunits (2).

The canonical ENaC is a heterotrimeric channel composed of three homologous subunits (α, β, and γ) (8). Each subunit has short intracellular N and C termini connected by a large extracellular loop. The extracellular loop probably represents a "handlike" structure, consisting of a "palm," "ball," "finger," "thumb," and "knuckle" domain (9). The extracellular loops of the α- and γ-subunits contain short inhibitory peptides in the finger domains, which are flanked by protease cleavage sites. The inhibitory peptide within the α-subunit is flanked by two cleavage sites that are recognized by the protease furin, whereas the inhibitory peptide within the γ-subunit contains only one furin cleavage site and additional cleavage sites for extracellular proteases (10). Furin, which is primarily present in the *trans*-Golgi network, cleaves the α-subunit twice and thereby releases its inhibitory peptide, whereas the γ-subunit is only cut once (2). Channels lacking this endogenous proteolytic maturation display a very low P_o, whereas furin-cleaved ENaCs that are translocated to the plasma membrane have moderate activity. Extracellular proteases cut the γ-subunit and thereby release its

The authors declare that they have no conflicts of interest with the contents of this article.

[1] Present address: Institute for Physiology and Pathophysiology, Vegetative Physiology, Philipps University of Marburg, 35037 Marburg, Germany.
[2] Present address: Institute for Anatomy and Cell Biology, Justus-Liebig University, 35392 Giessen, Germany.
[3] To whom correspondence should be addressed. Tel.: 44-191-208-4700; E-mail: Mike.Althaus@newcastle.ac.uk.

[4] The abbreviations used are: ENaC, epithelial sodium channel; DEG, degenerin; P_o, open probability; I_M, transmembrane current; V_M, membrane potential; MTSET, 2-(trimethylammonium)ethylmethanethiosulfonate; PNGase F, peptide–*N*-glycosidase F; HA, hemagglutinin; SSI, sodium self-inhibition; ANOVA, analysis of variance; bp, base pairs; TLCK, 1-chloro-3-tosylamido-7-amino-2-heptanone.

inhibitory peptide, resulting in ENaCs with a high P_o (2, 10). Proteolytic processing not only represents an additional level of ENaC regulation but was also suggested to be crucial for the transition of a stimulus-activated DEG/ENaC ancestor to a constitutively open channel during ENaC evolution (10).

In addition to the three subunits composing canonical ENaCs, a δ-subunit was identified, which can assemble with the β- and γ-subunits to form atypical ENaCs (11). The physiological importance of this subunit is not understood, but *in vitro* studies using human orthologues demonstrated that δβγ-ENaC has distinct properties from αβγ-ENaC (12). Complicating its physiological analysis, mice and rats lack a functional gene for δ-ENaC (13). However, δ-ENaC is present in amphibians, including the South African clawed frog *Xenopus laevis*, where it had originally been named ϵ-ENaC (14). Given the lack of an appropriate animal model to study this ion channel and the fact that *X. laevis* is an established model organism in molecular cell biology as well as physiology, this study investigated the molecular physiology of ENaC containing the δ-subunit in this species.

We demonstrate that δ-ENaC has a different expression pattern compared with α-ENaC and that δ-containing channels display an intrinsic dynamic open probability. We show that incorporation of the δ-subunit renders this amphibian ENaC completely insensitive to proteolytic activation by extracellular proteases due to intersubunit interactions involving γ-ENaC. We suggest that subunit composition provides an additional level of ENaC regulation but also propose that *Xenopus* δ-ENaC represents a functional example for ENaC at the interface of stimulus-activated and constitutively open DEG/ENaC ion channels, demonstrating the importance of proteolytic maturation in ENaC evolution.

Results

The δ-ENaC subunit is predominantly expressed in urogenital tissues in X. laevis

Due to the lack of specific antibodies that allow discrimination of α- and δ-ENaC, expression of these subunits was investigated in adult *X. laevis* via RT-PCR (Fig. 1). Control reactions were performed with cDNA samples that were generated without the addition of reverse transcriptase. These reactions were always negative and did not show any DNA signals in the MidoriGreen fluorescence of the agarose gels after the PCRs (data not shown). Transcripts for the δ-ENaC subunit were almost exclusively found in urogenital tissues (kidney, urinary bladder, testes, ovary, oocytes, and cloaca), whereas expression of the α-subunit was more diversely distributed (skin, lung, liver, parts of the gastrointestinal and urogenital tract, brain, and spinal cord). All δ-ENaC– expressing tissues, except the ovary, also contained transcripts for the α-subunit.

The presence of the δ-subunit alters ENaC characteristics

Functional characterization of αβγ- and δβγ-ENaC was achieved by expression of either channel isoform in *X. laevis* oocytes. Although transcripts for δ-ENaC were detected in oocytes (Fig. 1) injection of β- and γ-ENaC RNA does not produce amiloride-sensitive transmembrane current (I_M) (14), excluding a potential contamination by endogenous δ-ENaC.

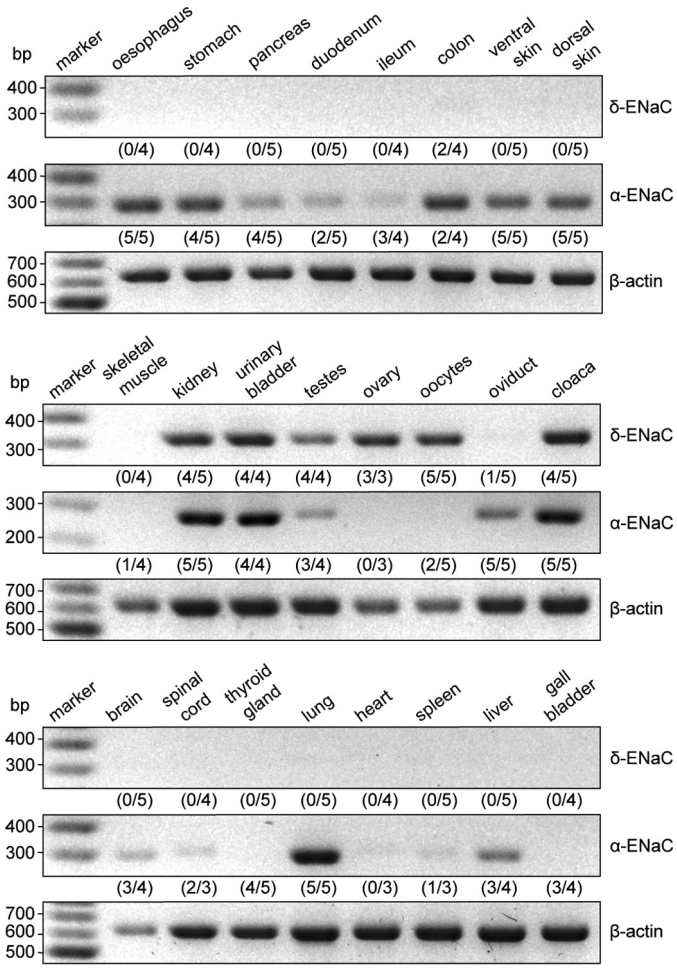

Figure 1. The δ-ENaC subunit is predominantly expressed in urogenital tissues in *X. laevis*. Tissues from adult *X. laevis* were screened for expression of δ- and α-ENaC subunit mRNA via RT-PCR. Amplicons for δ-ENaC (320 bp) were found in tissue samples from kidney, urinary bladder, testes, ovary, oocytes, and the cloaca. With the exception of the ovary, these tissues also expressed α-ENaC (291 bp). Amplification of β-actin mRNA (610 bp) served as a control. Control reactions have been performed without reverse transcriptase but are omitted from the figure for clarity. These reactions did not show any DNA signals in the MidoriGreen fluorescence of agarose gels after PCR. *Numbers* in *parentheses* indicate the quantity of positively tested samples with respect to the total amount of samples from different animals.

Electrophysiological assessment of whole-cell I_M at membrane potentials (V_M) from −100 to +40 mV revealed an inward current at negative V_M with a reversal potential of 9.8 mV (αβγ-ENaC) and 14.2 mV (δβγ-ENaC) and was inhibited by the ENaC-blocker amiloride (Fig. 2*a*). Consistent with previous reports (14), channel isoforms exhibited different kinetics of I_M after washout of amiloride. Cells expressing αβγ-ENaC display a slow and steady current increase that eventually reaches a plateau, whereas channels containing the δ-subunit show a rapid, peaked increase in I_M followed by a continuous current decline (Fig. 2*b*). Despite this current rundown, amiloride-sensitive current fractions (ΔI_{ami}) of δβγ-ENaC– expressing oocytes were 2.4-fold larger than in αβγ-ENaC– expressing cells (Fig. 2*c*). The increased ΔI_{ami} mediated by δβγ-ENaC was also sustained after 14 min when the current eventually approached a plateau (Fig. 2, *d* and *e*).

The increased ΔI_{ami} of δβγ-ENaC– expressing oocytes may result from changes in the single-channel conductance, P_o, or

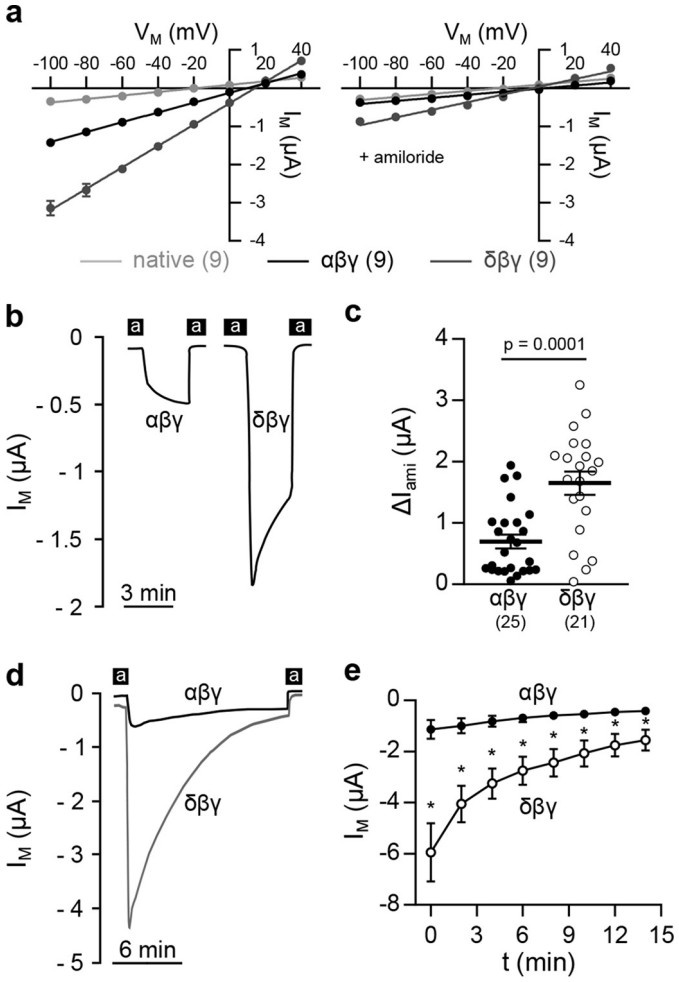

Figure 2. The δ-subunit alters ENaC characteristics. *a*, current (I_M)/voltage (V_M) plots of oocytes expressing $\alpha\beta\gamma$- or $\delta\beta\gamma$-ENaC in the absence (*left*) or presence (*right*) of amiloride. *b*, representative I_M recordings of oocytes expressing $\alpha\beta\gamma$- or $\delta\beta\gamma$-ENaC at −60 mV. *Black bars*, application of amiloride (*a*). *c*, amiloride-sensitive current fractions (ΔI_{ami}) in both ENaC isoforms derived from the second application of amiloride (Student's unpaired *t* test with Welch's correction). *d* and *e*, representative current traces (*d*) and corresponding mean values of I_M (*e*) of $\alpha\beta\gamma$- or $\delta\beta\gamma$-ENaC–expressing oocytes, depicting the enhanced current rundown of δ-ENaC–containing channels over an extended time period. At any given time point, I_M mediated by δ-containing channels was significantly increased compared with $\alpha\beta\gamma$-ENaC–mediated currents (*, $p < 0.0003$, Mann–Whitney *U* test). *Lines* and *error bars*, mean and S.E.

membrane abundance of these channels. Cell-attached patch-clamp recordings of oocytes expressing $\delta\beta\gamma$-ENaC revealed unitary channel characteristics similar to α-ENaC–containing channels (Fig. 3*a*). Analysis of individual recordings lasting for 120–180 s revealed no significant difference between ENaC isoforms in the number of visible channels or the slope conductance (G_{slope}), derived from V_M of −100 to −40 mV (Fig. 3, *b* and *c*). Although there was no difference in P_o compared with $\alpha\beta\gamma$-ENaC, channels containing the δ-subunit displayed significantly prolonged open times and a tendency for extended mean closed times that did not reach statistical significance (Fig. 3, *d* and *e*). Consistent with whole-cell currents (Fig. 2*d*), patch-clamp recordings of $\delta\beta\gamma$-ENaC regularly showed a decline of channel activity (Fig. 3*f*), which impaired proper estimation of P_o. Therefore, P_o of $\alpha\beta\gamma$- and $\delta\beta\gamma$-ENaC was additionally determined using 2-(trimethylammonium)ethylmethanethiosulfonate (MTSET)-sensitive β_{S540C}-ENaC mutant channels. Covalent modification of an introduced cysteine within the conserved degenerin site of β-ENaC by MTSET elevates P_o of ENaC containing the β_{S540C} mutation to 1.0 (16). Comparison of ΔI_{ami} before and after MTSET application allows estimation of channel P_o. The ΔI_{ami} of oocytes expressing $\alpha\beta_{S540C}\gamma$- or $\delta\beta_{S540C}\gamma$-ENaC was not significantly different from that for cells expressing respective WT channels (Fig. 4*a*). P_o of $\alpha\beta_{S540C}\gamma$- or $\delta\beta_{S540C}\gamma$-ENaC was estimated by measuring ΔI_{ami} before and after administration of MTSET (1 mM), which increased I_M mediated by both channels (Fig. 4, *b* and *c*), assuming that MTSET shifts the P_o of both channel isoforms to the same degree (close to 1.0). Although initial ΔI_{ami} of $\delta\beta_{S540C}\gamma$-ENaC was increased compared with α-ENaC–containing channels, this discrepancy was lost after application of MTSET (Fig. 4*d*). Comparison of the initial ΔI_{ami} with ΔI_{ami} after exposure to MTSET ($P_o = 1.0$) indicated a significantly larger initial P_o for ENaC containing the δ-subunit compared with $\alpha\beta_{S540C}\gamma$-ENaC (Fig. 4*e*). Overall, these data suggest that the presence of the δ-subunit enhances the amount of current generated by ENaC due to an increased P_o rather than single-channel conductance, but also changes current into a transient form.

The δ-subunit is not proteolytically processed and does not change membrane abundance compared with α-containing channels

Proteolytic processing of ENaC subunits by intra- and extracellular proteases impacts channel P_o (10). To monitor proteolytic cleavage of both $\alpha\beta\gamma$- and $\delta\beta\gamma$-ENaC, epitope-tagged $\alpha_{HA/V5}$- and $\delta_{HA/V5}$-ENaC subunits containing an N-terminal HA tag and a C-terminal V5 tag were generated (Fig. 5*a*). Immunoblots from whole-cell lysates of oocytes expressing either $\alpha_{HA/V5}\beta\gamma$- or $\delta_{HA/V5}\beta\gamma$-ENaC targeted against the HA or V5 tag revealed a discrepancy in the endogenous cleavage pattern of both ENaC subunits (Fig. 5*b*). Blots targeting the N-terminal HA tag of the $\alpha_{HA/V5}$-subunit displayed a full-length peptide at ~75 kDa and two short peptides at ~18 and ~13 kDa, probably corresponding to cleavage products resulting from proteolysis by intracellular furin, which cuts the α-subunit twice (*Xenopus* α-ENaC: $RVKR^{145}$ and $RVSR^{168}$) (17). In contrast, only the full-length peptide of the $\delta_{HA/V5}$-subunit at ~75 kDa was detected, consistent with the lack of a minimal consensus sequence for furin-mediated cleavage (RXXR↓ (18)) in this ENaC subunit. These findings were confirmed by blots targeting the C-terminal V5 tags, which yielded two signals for $\alpha_{HA/V5}$-ENaC, representing full-length (~75 kDa) and cleaved (~60 kDa) peptides but only one signal (~75 kDa) representing the full-length $\delta_{HA/V5}$-ENaC. Proteolysis by furin would occur in the *trans*-Golgi network. Therefore, glycosylation of the $\delta_{HA/V5}$-subunit, which is also associated with this route for post-translational modification, was examined. Treatment of whole-cell lysates from oocytes expressing $\delta_{HA/V5}\beta\gamma$-ENaC with PNGase F induced a downward migration shift of the signal in blots targeting the V5 tag (Fig. 5*c*). This indicates glycosylation of the δ-ENaC subunit and suggests passage through the *trans*-Golgi network. Epitope-tagged $\alpha_{HA/V5}$- and $\delta_{HA/V5}$-ENaC subunits were subsequently employed to compare membrane abundance of both channel isoforms by

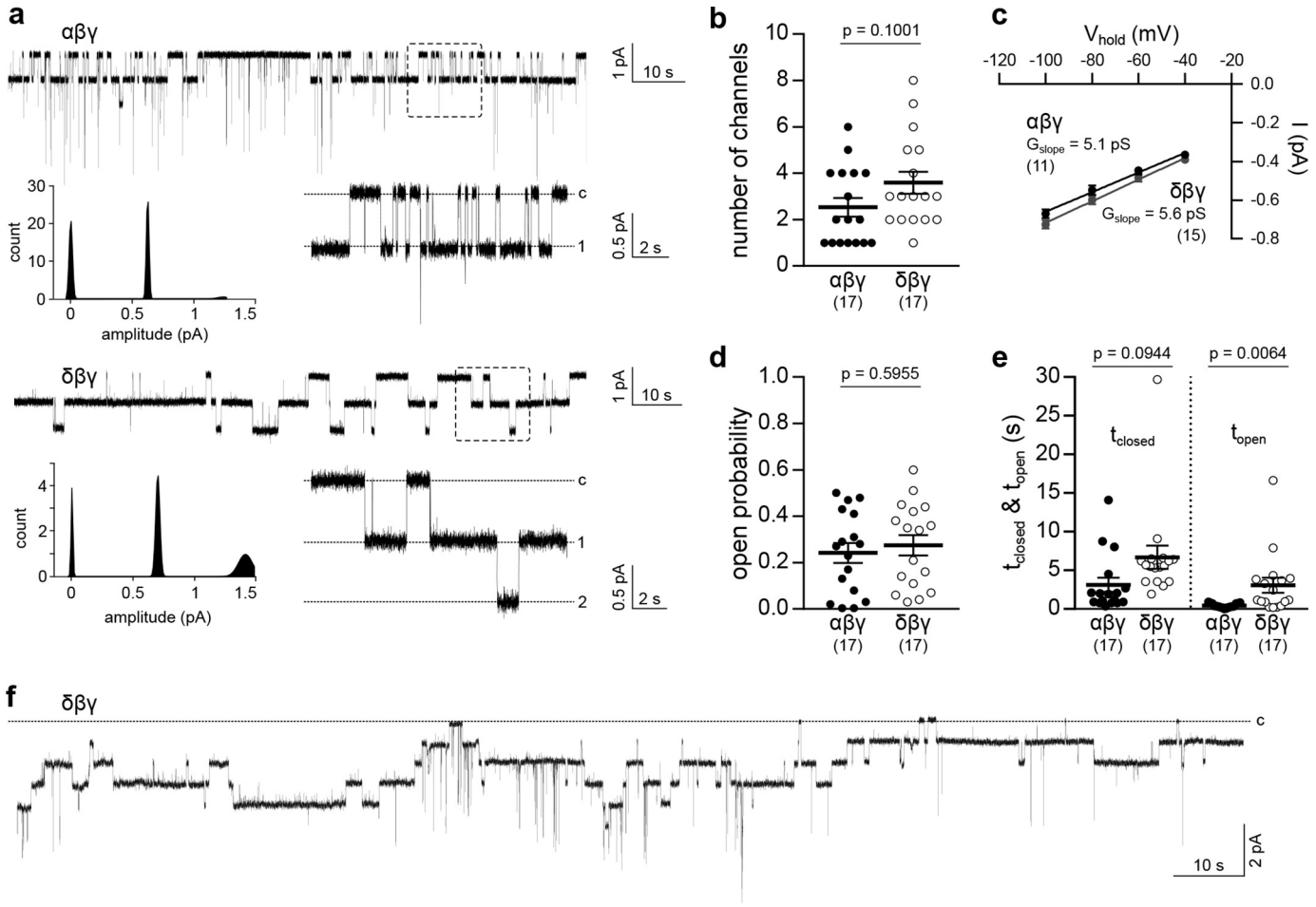

Figure 3. *Xenopus* $\alpha\beta\gamma$- and $\delta\beta\gamma$-ENaC single-channel characteristics. *a*, representative current traces from cell-attached patch-clamp recordings of $\alpha\beta\gamma$- or $\delta\beta\gamma$-ENaC–expressing oocytes ($V_M = -100$ mV). Amplitude histograms depict Gaussian distribution of channel amplitudes. *Dotted squares*, areas of trace magnification (*c*, closed; *1*, *2*, number of open channels). *b*, number of visible channels in cell-attached recordings as presented in *a* (Student's unpaired *t* test). *c*, slope conductance (G_{slope}) of $\alpha\beta\gamma$- and $\delta\beta\gamma$-ENaC derived from linear regression of unitary channel conductance at −40 to −100 mV. *d*, apparent open probability of both ENaC isoforms (Student's unpaired *t* test). *e*, estimation of single-channel kinetics revealed an increased open time (t_{open}) of $\delta\beta\gamma$-ENaC, but no significant change in closed time (t_{closed}) between ENaC isoforms (Dunn's multiple-comparison test). Evaluation of all single-channel characteristics was performed using current recordings with a duration of 120–180 s with a maximum of eight channels per patch. *f*, cell-attached recording of a $\delta\beta\gamma$-ENaC–expressing oocyte indicating a rundown of ENaC activity that impedes a precise determination of channel open probability. *Lines* and *error bars*, mean and S.E.

surface biotinylation. Similar to WT channels, the ΔI_{ami} mediated by $\delta_{HA/V5}\beta\gamma$-ENaC was increased compared with $\alpha_{HA/V5}\beta\gamma$-ENaC (Fig. 5, *d* and *e*). Only a single signal (~60 kDa) was detected in membrane fractions from $\alpha_{HA/V5}\beta\gamma$-ENaC–expressing cells, indicating the absence of unprocessed $\alpha_{HA/V5}$-ENaC peptides at the cell surface, whereas only unprocessed $\delta_{HA/V5}$-ENaC peptides (~75 kDa) could be detected in membrane and cytosolic fractions (Fig. 5*f*). Membrane abundance was determined by densitometric analysis of signal intensities from both membrane and cytosolic protein fractions in V5-targeted immunoblots. There was no difference in surface expression between $\alpha_{HA/V5}\beta\gamma$- and $\delta_{HA/V5}\beta\gamma$-ENaC (Fig. 5*g*), supporting the notion that an enhanced P_o rather than membrane abundance contributes to the increased I_M mediated by ENaC containing the δ-subunit. In sum, these data suggest that unlike α-ENaC, the δ-subunit does not undergo proteolytic maturation by the endogenous protease furin, and incorporation of this subunit does not affect channel membrane abundance.

ENaCs containing the δ-subunit are insensitive to activation by extracellular proteases

Because the δ-ENaC subunit is not processed by furin, the activation of $\alpha\beta\gamma$- and $\delta\beta\gamma$-ENaC by extracellular proteases was compared. Oocytes expressing either ENaC isoform were exposed to chymotrypsin, which activates ENaC at the cell surface (19). The ΔI_{ami} of both channel isoforms was determined before and after perfusion of the cells with 2 μg/ml α-chymotrypsin (from bovine pancreas, TLCK-treated; Sigma) in ORS (90 mM NaCl, 1 mM KCl, 2 mM $CaCl_2$, 5 mM HEPES, pH 7.4) containing amiloride for 5 min (Fig. 6, *a* and *d*). Administration of chymotrypsin significantly increased ΔI_{ami} of oocytes expressing $\alpha\beta\gamma$-ENaC (Fig. 6*b*). This activation was also present in cells incubated with furin inhibitor I (40 μM) before recordings. Inhibition of furin potentiated the proteolytic activation of $\alpha\beta\gamma$-ENaC from a 4-fold to a 9-fold increase of ΔI_{ami}, whereas no change of ΔI_{ami} (-fold activation = 1) was observed in control groups that were perfused with ORS containing amiloride without chymotrypsin (Fig. 6*c*). Application of chy-

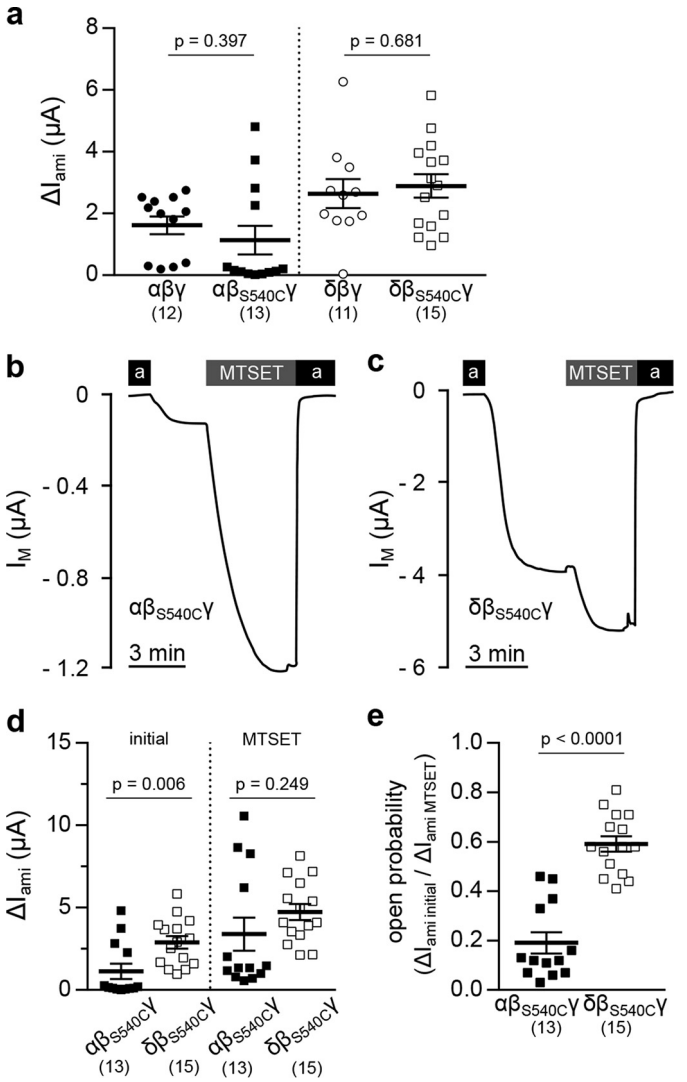

Figure 4. The MTSET-sensitive β_{S540C}-ENaC mutant reveals an increased open probability of ENaCs containing the δ-subunit. *a*, amiloride-sensitive current fractions (ΔI_{ami}) of oocytes expressing $\alpha\beta\gamma$- or $\delta\beta\gamma$-ENaC containing either WT β-ENaC or the β_{S540C}-ENaC mutation (Student's unpaired *t* test). *b* and *c*, representative I_M traces of oocytes expressing $\alpha\beta_{S540C}\gamma$- or $\delta\beta_{S540C}\gamma$-ENaC. The open probability of both channel isoforms was determined by assessing ΔI_{ami} before and after the application of MTSET (1 mM). *d*, statistical comparison of ΔI_{ami} of oocytes expressing $\alpha\beta_{S540C}\gamma$- or $\delta\beta_{S540C}\gamma$-ENaC before (initial) and after application of MTSET (*initial*, Student's unpaired *t* test; *MTSET*, Student's unpaired *t* test with Welch's correction). *e*, open probability of $\alpha\beta_{S540C}\gamma$- and $\delta\beta_{S540C}\gamma$-ENaC determined by the ratio of $\Delta I_{ami\ initial}$/$\Delta I_{ami\ MTSET}$ (Student's unpaired *t* test). *Lines* and *error bars*, mean and S.E.

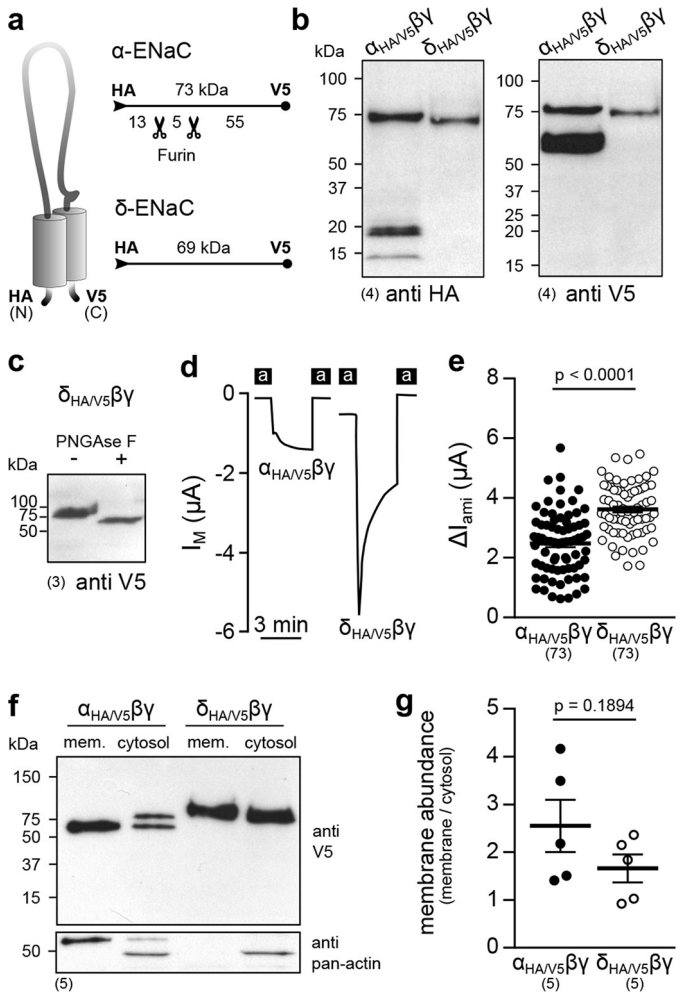

Figure 5. The δ-subunit is not subject to proteolytic maturation, and $\delta\beta\gamma$-ENaC membrane abundance is not changed compared with α-containing channels. *a*, schematic depiction of epitope-tagged ENaC subunits. The *numbers* indicate approximate molecular mass of peptides with/without furin cleavage, detected by immunoblots, as presented in *b*. *b*, immunoblots of whole-cell lysates from oocytes expressing $\alpha_{HA/V5}\beta\gamma$- or $\delta_{HA/V5}\beta\gamma$-ENaC using anti-HA and anti-V5 antibodies. *c*, a migration shift of the $\delta_{HA/V5}$-subunit due to treatment with PNGase F indicates glycosylation of the protein. *d*, representative I_M recordings of oocytes expressing $\alpha_{HA/V5}\beta\gamma$- or $\delta_{HA/V5}\beta\gamma$-ENaC. *e*, amiloride-sensitive current fractions (ΔI_{ami}) of $\alpha_{HA/V5}\beta\gamma$- and $\delta_{HA/V5}\beta\gamma$-ENaC (Student's unpaired *t* test). *f*, immunoblot using an anti-V5-antibody of membrane (*mem.*) and cytosolic fractions from oocytes expressing $\alpha_{HA/V5}\beta\gamma$- or $\delta_{HA/V5}\beta\gamma$-ENaC. The *bottom blot* shows the results from reprobing of the same membrane with an anti-pan-actin antibody to verify proper fractionation. *g*, membrane abundance of $\alpha_{HA/V5}\beta\gamma$- and $\delta_{HA/V5}\beta\gamma$-ENaC derived from densitometric analysis of immunoblots as shown in *f* (Student's unpaired *t* test). *Lines* and *error bars*, mean and S.E.

motrypsin did not increase currents mediated by $\delta\beta\gamma$-ENaC, regardless of preceding incubation with the furin inhibitor (Fig. 6, *d–f*). The same results were observed using trypsin (data not shown). These data indicate that currents generated by $\delta\beta\gamma$-ENaC are insensitive to activation by extracellular serine proteases, such as chymotrypsin and trypsin.

The presence of the δ-subunit prevents cleavage of the γ-subunit by extracellular proteases

Intracellular cleavage of the γ-ENaC subunit renders the channel susceptible to activation by extracellular proteases (20). Cleavage of γ-ENaC at the cell surface by extracellular proteases induces the release of its inhibitory peptide and activates the channel (21). Because the δ-subunit prevented ENaC activation by extracellular chymotrypsin, the cleavage states of the α-, δ-, and γ-subunits at successive stages of proteolytic ENaC processing were examined. Epitope-tagged subunits were expressed in oocytes together with WT ENaC subunits ($\alpha_{HA/V5}\beta\gamma$, $\delta_{HA/V5}\beta\gamma$, $\alpha\beta\gamma_{HA/V5}$, and $\delta\beta\gamma_{HA/V5}$), and ΔI_{ami} of individual oocytes from each group with or without prior incubation in chymotrypsin (2 μg/ml; 5 min) was measured. After surface biotinylation, membrane fractions were isolated, and cleavage states of individual ENaC subunits were analyzed in immunoblots targeted at the C-terminal V5 epitope. Incubation with chymotrypsin enhanced ΔI_{ami} of $\alpha_{HA/V5}\beta\gamma$-ENaC–

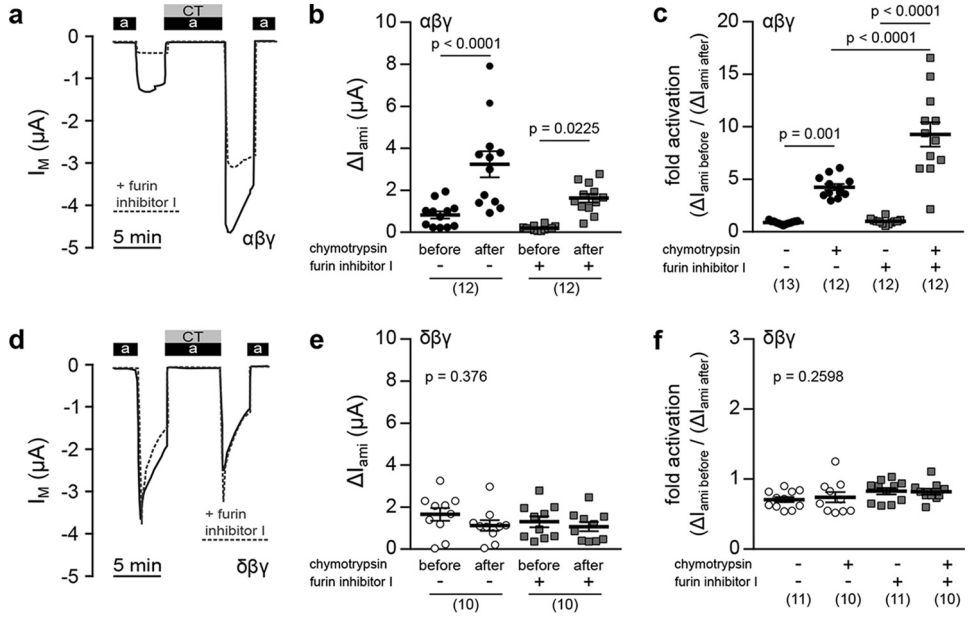

Figure 6. ENaCs containing the δ-subunit are insensitive to activation by extracellular proteases. *a*, representative I_M traces of oocytes expressing αβγ-ENaC. Proteolytic channel activation was determined by assessing amiloride-sensitive current fractions (ΔI_{ami}) before and after application of chymotrypsin (*CT*; 2 μg/ml) together with amiloride (*a*). Current traces of oocytes previously incubated with furin inhibitor I (40 μM) are depicted as *dotted gray lines*. *b*, comparison of ΔI_{ami} before and after application of chymotrypsin in oocytes incubated with (+) or without (−) furin inhibitor I (one-way ANOVA; $F = 15.31$, $p < 0.0001$; Tukey's multiple comparison test). *c*, comparison of -fold activation in ΔI_{ami} between experimental groups (*chymotrypsin* +) and control groups (*chymotrypsin* −) (one-way ANOVA; $F = 44.4$, $p < 0.0001$; Tukey's multiple comparison test). *d–f*, I_M traces (*d*) and statistical evaluation of changes in ΔI_{ami} in oocytes expressing δβγ-ENaC. Data presentation is equivalent to *a–c*. *e*, Kruskal–Wallis test, $p = 0.376$; Dunn's multiple-comparison test. *f*, one-way ANOVA; $F = 1.393$, $p = 0.2598$; Tukey's multiple-comparison test. *Lines* and *error bars*, mean and S.E.

expressing oocytes, whereas this activation was absent in $\delta_{HA/V5}\beta\gamma$-ENaC–expressing cells (Fig. 7*a*). In corresponding immunoblots, two signals at ~75 and ~60 kDa were visible in cytosolic fractions for the $\alpha_{HA/V5}$-ENaC subunit that represent uncleaved and furin-cleaved peptides, whereas only processed subunits were present in membrane fractions (Fig. 7*b*). Analogous stages of subunit maturation were not observed for the $\delta_{HA/V5}$-subunit, for which only one signal at ~75 kDa was visible in cytosolic and membrane fractions. No additional cleavage products of $\alpha_{HA/V5}$- and $\delta_{HA/V5}$-ENaC were found in membrane fractions of chymotrypsin-treated oocytes, indicating no further subunit cleavage at the cell surface. However, examination of $\gamma_{HA/V5}$-ENaC cleavage stages revealed further processing of this subunit at the cell surface, which depended on its co-expression with α- or δ-ENaC. Whereas ΔI_{ami} mediated by $\alpha\beta\gamma_{HA/V5}$-ENaC was increased in oocytes treated with chymotrypsin, activity of $\delta\beta\gamma_{HA/V5}$-ENaC was unaffected by the protease (Fig. 7*c*). Immunoblots of either α- or δ-ENaC–containing channels revealed two signals in cytosolic fractions that represent uncleaved (~100-kDa) and cleaved (~75-kDa) $\gamma_{HA/V5}$-ENaC peptides (Fig. 7*d*). Only one signal was present in the membrane fraction of these cells (~75 kDa), indicating the absence of uncleaved $\gamma_{HA/V5}$-ENaC subunits at the cell surface. An additional cleavage product (~70 kDa) appeared in the membrane fraction of $\alpha\beta\gamma_{HA/V5}$-ENaC–expressing oocytes after incubation with chymotrypsin. However, chymotrypsin did not induce an additional cleavage product in membrane fractions of cells expressing $\delta\beta\gamma_{HA/V5}$-ENaC. The secondary cut of $\gamma_{HA/V5}$-ENaC by chymotrypsin is prevented in the presence of the δ-subunit, which probably contributes to the insensitivity of δβγ-ENaC to extracellular proteases. These data indicate that the presence of the δ-subunit prevents cleavage of the γ-subunit at the cell surface and activation by extracellular proteases.

Discussion

This study revealed that the presence of the δ-subunit changes properties of transmembrane currents generated by *X. laevis* ENaC. In contrast to the rather stable currents mediated by αβγ-ENaC, channels containing the δ-subunit mediated larger currents that had a more transient nature. These observations are consistent with findings from a previous study and can be attributed to differences in the speed of ENaC sodium self-inhibition (SSI) (14), which reflects the allosteric reduction of ENaC P_o in the presence of extracellular sodium ions (5). SSI kinetics are reduced in *Xenopus* ENaCs containing the δ-subunit (14). Human δβγ-ENaC also displays a slow progression of SSI (22) and reduced gating kinetics (11), suggesting a generally decreased gating velocity of ENaC containing the δ-subunit. This is supported by single-channel recordings of both ENaC isoforms presented in this study, which revealed prolonged mean open times and a tendency for longer closed times of δ-containing ENaCs. However, whereas the magnitude of SSI is decreased in human δβγ-ENaC (22), it is markedly pronounced in the *Xenopus* orthologue (14) and probably accounts for the rather transient current form observed for δβγ-ENaC in this study.

Despite this rundown, whole-cell currents of oocytes expressing δβγ-ENaC were consistently larger compared with αβγ-ENaC–expressing cells. Similarly, substitution of α- for the δ-subunit in human ENaC results in elevated whole-cell currents, which have been suggested to be caused by a larger

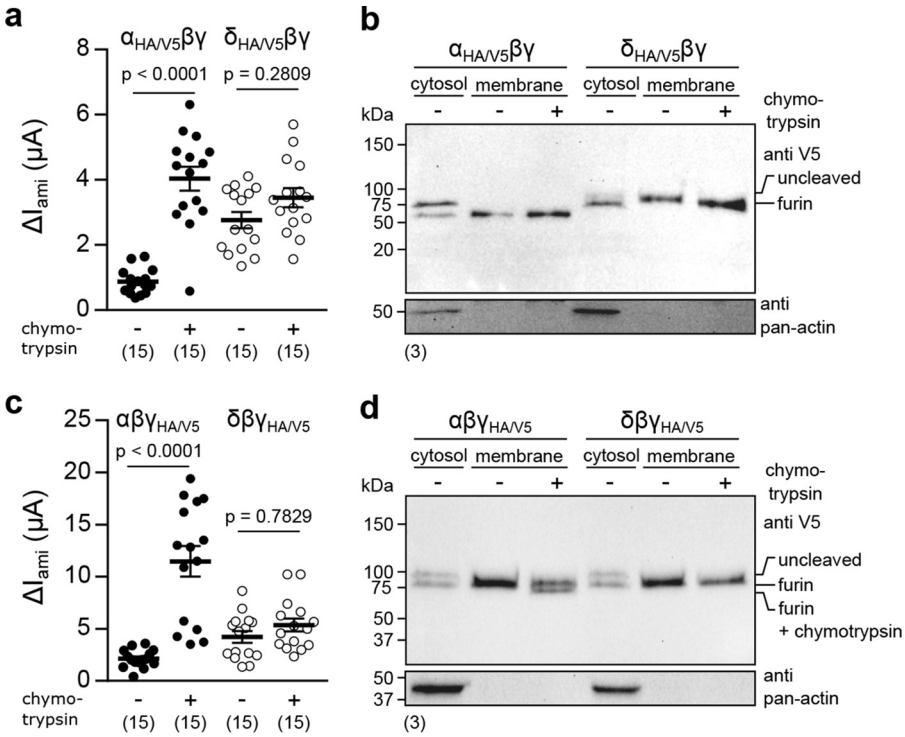

Figure 7. The presence of the δ-ENaC subunit prevents cleavage of the γ-subunit by extracellular proteases. *a*, comparison of ΔI_{ami} from oocytes expressing epitope-tagged $\alpha_{HA/V5}\beta\gamma$- or $\delta_{HA/V5}\beta\gamma$-ENaC with (+) or without (−) prior incubation with chymotrypsin (2 μg/ml, 5 min). *b*, V5-targeted immunoblots of cytosolic and membrane fractions from oocytes expressing $\alpha_{HA/V5}\beta\gamma$- or $\delta_{HA/V5}\beta\gamma$-ENaC that were treated with (+) or without (−) chymotrypsin. Blots were reprobed for pan-actin to verify proper isolation of membrane fractions. *c*, ΔI_{ami} of oocytes expressing epitope-tagged $\alpha\beta\gamma_{HA/V5}$- or $\delta\beta\gamma_{HA/V5}$-ENaC with (+) or without (−) prior incubation with chymotrypsin. *d*, V5-targeted immunoblots of cytosolic and membrane fractions from oocytes expressing $\alpha\beta\gamma_{HA/V5}$- or $\delta\beta\gamma_{HA/V5}$-ENaC, which were treated with (+) or without (−) chymotrypsin. *Lines* and *error bars*, mean and S.E.

single-channel conductance and an enhanced P_o (19). Channels resulting from co-expression of *Xenopus* δ-ENaC with the human β- and γ-ENaC subunits also exhibit a high spontaneous P_o, whereas their unitary conductance equaled those of α-ENaC–containing channels (23). Cell-attached patch-clamp recordings of *Xenopus* α- and δβγ-ENaC in the present study did not reveal differences in the conductance or P_o of these ENaC isoforms, supporting the concept that incorporation of the δ-ENaC subunit from *X. laevis* does not affect ENaC single-channel conductance. Without apparent differences in the number of visible channels and P_o of αβγ- and δβγ-ENaC obtained from patch-clamp recordings, the observed differences in amiloride-sensitive whole-cell currents could not be explained. A continuous decrease of channel activity was observed in patches containing δβγ-ENaC, which corresponds to the macroscopic decline of whole-cell transmembrane currents due to SSI and suggests an SSI-dependent temporal decrease in channel activity.

Alternative determination of P_o at the whole-cell level using mutant β_{S540C}-ENaC in combination with MTSET displayed a markedly increased P_o of δ-ENaC compared with α-ENaC–containing channels. The generated *Xenopus* β_{S540C}-ENaC mutation is analogous to the previously utilized rat β_{S518C} (24) and human β_{S520C} (19) constructs that target the conserved "degenerin" site of ENaC subunits, which corresponds to a domain essential for the gating of related DEG channels in *Caenorhabditis elegans* (25). Administration of MTSET to ENaC containing this mutation sets channel P_o to nearly 1.0 through the covalent addition of a bulky residue to the introduced cysteine near the channel gate (16), and we assumed that MTSET shifts the P_o of α- and δ-containing ENaCs to the same degree. Introduction of this mutation did not change baseline ENaC current, as initial ΔI_{ami} of channels containing the mutant β_{S540C}-subunit were not significantly different from respective WT channels. MTSET increased ΔI_{ami} of $\alpha\beta_{S540C}\gamma$-ENaC and, to a lower extent, ΔI_{ami} of $\delta\beta_{S540C}\gamma$-ENaC. Assuming a similarly effective activation of both ENaC isoforms by MTSET and a negligible proportion of closed channels that are insensitive to chemical modification (16), the estimated P_o of $\alpha\beta_{S540C}\gamma$-ENaC (0.2) correlates well to patch-clamp results in this (0.24) and a previous study (7). ENaC containing the δ-subunit displayed a P_o that was 3 times larger (0.6), which explains the enhanced whole-cell currents mediated by *Xenopus* δβγ-ENaC. Furthermore, equal levels of ΔI_{ami} in α- and $\delta\beta_{S540C}\gamma$-ENaC after application of MTSET indicate a similar membrane expression of both channel isoforms. This is further supported by the equal number of visible channels observed in patch-clamp recordings of α- and δβγ-ENaC as well as the similar membrane abundance of epitope-tagged $\alpha_{HA/V5}$- or $\delta_{HA/V5}$-ENaC subunits. Hence, an elevated P_o is the major determinant for increased whole-cell currents mediated by δβγ-ENaC, but P_o is not stable and decreases over time.

Interestingly, introduction of the β_{S540C} mutation abolished the transient nature of whole-cell currents mediated by δ-containing ENaC. This supports the conclusion that the transient activity of *Xenopus* δβγ-ENaC reflects its P_o, which is inhibited in the presence of extracellular sodium due to SSI. As a release from SSI and a resulting increase of ENaC P_o are essential for

channel activation by proteolytic processing (26), the regulation of *Xenopus* δβγ-ENaC by proteases was investigated.

Initial proteolytic processing of ENaC occurs by selective cleavage of the α- and γ-ENaC subunits by furin (27). During this proteolytic maturation in the *trans*-Golgi network, furin cleaves the channel at three distinct sites. Two cleavage sites located in the finger domain of α-ENaC enclose a small inhibitory peptide that is released upon furin-mediated cleavage (28), whereas proteolysis at a single site on the γ-ENaC subunit primes the channel for further activation at the cell surface (20). Secondary proteolysis of the γ-ENaC subunit distal to the furin cleavage site entails the dissociation of another inhibitory peptide and thus facilitates activation of ENaC at the cell surface by further increasing P_o. Additional cleavage of γ-ENaC may be facilitated by various serine proteases like trypsin, channel-activating protease 1, or neutrophil elastase (2).

The present study demonstrates that the δ-subunit of *Xenopus* ENaC is not subject to proteolytic maturation by furin, and channels containing this subunit are insensitive to activation by extracellular proteases. Immunoblots targeting epitope-tagged $\alpha_{HA/V5}$-, $\delta_{HA/V5}$-, or $\gamma_{HA/V5}$-ENaC subunits revealed α- and γ-ENaC cleavage fragments. These fragments probably represent furin cleavage products, because both ENaC subunits contain conserved furin consensus sites (R*XX*R ↓) (2), and channel activation by extracellular chymotrypsin is potentiated after inhibition of furin. By contrast, the absence of δ-ENaC cleavage fragments in oocyte whole-cell lysates and membrane fractions implies a lack of intracellular proteolytic processing and is consistent with the absence of a furin consensus site in the peptide sequence of this subunit. Furthermore, the stimulatory effect of extracellular proteases as observed for αβγ-ENaC was completely lost in δβγ-ENaC. Immunoblots targeting the V5 epitope of $\gamma_{HA/V5}$-ENaC revealed two signals, corresponding to uncleaved and furin-cleaved peptides, in cytosolic fractions, whereas the membrane fraction only contained one signal corresponding to the furin-cleaved peptide. This was observed for $\gamma_{HA/V5}$-ENaC after co-expression with the α- or δ-subunit, suggesting that the presence of the δ-subunit does not prevent intracellular maturation of γ-ENaC. After exposure to chymotrypsin, an additional immunoblot signal occurred in membrane fractions of $\alpha\beta\gamma_{HA/V5}$-ENaC, representing a second cleavage event in the γ-subunit by the extracellular protease. In contrast, this was not observed in $\delta\beta\gamma_{HA/V5}$-ENaC, suggesting that the presence of the δ-subunit prevents cleavage of γ-ENaC by extracellular proteases. Extracellular cleavage of the γ-subunit is considered rate-limiting for maximal ENaC activation at the cell surface, thus explaining the lack of functional current stimulation of δβγ-ENaC by chymotrypsin.

The lack of an ENaC crystal structure complicates the mechanistic interpretation of this observation. The crystal structure of the homologous acid–sensing ion channel suggests that the finger domains play a prominent role in intersubunit interactions (9). Based on the location of the inhibitory peptides within the finger domains of the α- and γ-subunit (2), it could be hypothesized that cleavage of the α-subunit triggers structural changes that affect the neighboring γ-subunit. The lack of cleavage in the δ-subunit might prevent such a structural rearrangement and prevent extracellular proteases from accessing corresponding cleavage sites in the γ-subunit. This hypothesis is challenged by the fact that the presence of the inhibitory sequence rather than cleavage *per se* is responsible for low ENaC activity (2). However, the peptide sequence of the δ-subunit does not contain homologies to an inhibitory tract, and activity of δβγ-ENaC is generally higher than that of αβγ-ENaC. The lack of an inhibitory peptide in δ-ENaC might therefore lead to an enhanced ENaC P_o, but also prevent further increase in P_o by impeding the access of extracellular proteases to the γ-subunit.

The lack of proteolytic processing might also be reflected in the observed expression pattern of α- and δ-ENaC in *Xenopus* tissues. Protease/anti-protease balance is suggested as a mechanism regulating the volume of surface liquid lining pulmonary epithelia (29). This might explain the need for a protease-sensitive ENaC in lung epithelia and the lack of δ-ENaC in this organ. The presence of δ-ENaC in osmoregulatory organs, such as the kidney, might constitute an additional level of ENaC control, bypassing proteolytic regulation. Future studies will have to identify the precise cellular localization of α- and δ-ENaC as well as the mechanisms regulating the expression and P_o of δβγ-ENaC. Interestingly, δ-ENaC mRNA was detected in testes and oocytes/ovaries. Because experimental expression of the *Xenopus* ENaC β- and γ-subunits does not increase transmembrane currents in oocytes (14), which would occur due to complementation of the channel by endogenous δ-ENaC, it is likely that translation of (maternal) δ-ENaC mRNA is blocked by masking proteins (30). This, however, might suggest a role for δ-ENaC in early embryonic development. Extracellular serine proteases play an important role in *Xenopus* early embryonic development (31); a functional role for ENaC channels in embryogenesis, however, remains to be proven.

Finally, the data reported herein may provide insights into ENaC evolution. Kleyman's group suggested that proteolytic processing was a crucial step in the evolution of ENaC from a stimulus-activated DEG/ENaC ancestor to a constitutively open channel (10) and hence adaptation to terrestrial life. Unlike any other vertebrate ENaC characterized to date, *Xenopus* δ-ENaC is the only channel that is completely insensitive to proteolytic processing and also the only vertebrate ENaC that displays a strong current rundown that is almost comparable with transient currents triggered by acid–sensing ion channels, which are evolutionarily older than ENaC. Furthermore, *Xenopus* δ-ENaC is the only α-like subunit that does not generate currents when expressed alone in oocytes (14). *Xenopus* δ-ENaC might therefore provide functional evidence for Kleyman's hypothesis of proteolytic activation as a prerequisite for constitutively open ENaCs. Interestingly, cloning of three ENaC subunits from the Australian lungfish, *Neoceratodus forsteri*, revealed the presence of furin cleavage sites in the γ-subunit, but not in the α-subunit (32). Because lungfish are the oldest living ancestors of tetrapods, proteolytic sensitivity of the γ-subunit might have been a prerequisite for further evolution of proteolytic maturation in α-like ENaC subunits in higher tetrapods.

Overall, our findings suggest that subunit composition constitutes an additional level of ENaC regulation, and we propose that the *Xenopus* δ-ENaC subunit represents a functional

example that demonstrates the importance of proteolytic maturation during ENaC evolution.

Experimental procedures

Isolation of X. laevis tissues

All procedures and experimental protocols were approved by the Animal Welfare Officer of the University of Giessen (registration number M_478/M_549) as well as the Animal Welfare and Ethical Review Body at Newcastle University (project ID 630). The animal housing facility (Giessen, Germany) was licensed by local authorities (Az: FD 62-§11 JLU Tierphysiologie). The methods used to humanely euthanize the animals were consistent with the recommendations of the AVMA Guidelines for the Euthanasia of Animals. Adult *X. laevis* were anesthetized for 15 min in 0.2% MS-222/H_2O (Pharmaq, New Hampshire, UK) at pH 6 and euthanized by decapitation and sounding of the spinal cord. Tissue samples used for RNA isolation were removed and immediately transferred into RNAlater solution (Qiagen, Hilden, Germany). Oocytes were isolated exactly as described previously (7) and kept in culture oocyte Ringer's solution (CulORS: 90 mM NaCl, 1 mM KCl, 2 mM $CaCl_2$, 5 mM HEPES, 2.5 mM sodium pyruvate, 0.06 mM penicillin G, and 0.02 mM streptomycin sulfate, pH 7.4). For some experiments, oocytes were purchased from the European *Xenopus* Resource Centre (Portsmouth, UK) or Ecocyte Bioscience (Castrop-Rauxel, Germany).

RNA isolation and RT-PCR

Total mRNA pools were isolated from *X. laevis* tissue samples employing the RNeasy extraction system (Qiagen, Hilden, Germany) according to the manufacturer's instructions. The mRNA was reverse-transcribed in cDNA using a poly(A) primer together with the ImProm-II reverse transcription system (Promega, Mannheim, Germany). For controls, identical reactions were performed without reverse transcriptase. The cDNA served as a template in a PCR (GoTaq DNA polymerase kit, Promega) using primers listed in Table 1. PCR conditions were an initial denaturation at 95 °C for 5 min, followed by 35 cycles of denaturation at 95 °C for 45 s, annealing at 64 °C for 30 s, and elongation at 72 °C for 45 s. The reaction was terminated with a final extension at 72 °C for 10 min. Amplicons were separated on a 1% agarose gel and visualized by MidoriGreen (Nippon Genetics, Dueren, Germany) fluorescence.

Table 1
Primer sequences used for RT-PCR

Target	Primer sequence (5′–3′)	Amplicon
		bp
α-ENaC		
Forward	AGCAGGTCTGTGTCCGTTCT	291
Reverse	ATTGTCGGGACAGTGTGTGA	
δ-ENaC		
Forward	ACCACTTTCTGGCTTGTGCT	320
Reverse	CCTCCATTGACTTGGCCTGT	
β-Actin		
Forward	GCCCGCATAGAAAGGAGACA	610
Reverse	GTCTGTCAGGTCACGTCCAG	

Plasmids and cRNA synthesis

Coding sequences for *X. laevis* δ-, α-, β-, and γ-ENaC were present in the pTNT expression vector (Promega). A MTSET-sensitive β_{S540C}-ENaC mutant was generated by site-directed mutagenesis (primers listed in Table 2) using the QuikChange Lightning Kit (Agilent Technologies, Waldbronn, Germany) according to the manufacturer's instructions. The δ-, α-, and γ-ENaC subunits were tagged with an HA epitope (YPYDVPDYA) at the N terminus and a V5 epitope (GKPIPNPLLGLDST) at the C terminus by PCR, using extended primers (Table 2) and Platinum Pfx DNA polymerase (Invitrogen, Karlsruhe, Germany). PCR was performed by initial denaturation for 5 min at 95 °C, followed by 35 cycles of denaturation for 45 s at 95 °C, annealing for 30 s at 70 °C, and elongation for 180 s at 72 °C. The reaction was terminated by elongation for 10 min at 72 °C, and amplicons were separated on 0.8% agarose gels. Bands of appropriate sizes were purified using a Gelextract minikit (5Prime, Darmstadt, Germany), and A-overhangs (3′) were generated employing the GoTaq DNA polymerase system (Promega). Amplicons were ligated (T4 Ligase, Promega) into the pGEM-T_{easy} vector (Promega) according to the manufacturer's protocol and transformed into competent *Escherichia coli* (K12, DH5α). Transformed clones were identified by ampicillin resistance and blue/white selection. Plasmids were isolated employing the QIAprep Spin Miniprep kit (Qiagen) and cut using restriction enzymes (XhoI/XbaI for δ-ENaC, SalI/NotI for α- and γ-ENaC; Promega). Fragments were separated on 0.8% agarose gels, and bands of appropriate sizes were purified (Gelextract Mini Kit; 5Prime) and ligated (T4 Ligase, Promega) into pTNT. All plasmids were sequenced (SeqLab, Goettingen, Germany) to verify successful mutagenesis and epitope tagging.

Plasmids encoding δ- and α-ENaC were linearized with BamHI, and plasmids encoding γ-ENaC were linearized with NaeI (both from Promega). Plasmids containing β-ENaC were not linearized due to the presence of BamHI and NaeI restriction sites in the DNA sequence. m^7G-capped cRNA was generated by *in vitro* transcription using T7 RNA polymerase (RiboMAX large-scale RNA production system, Promega) according to the manufacturer's protocol. cRNAs were diluted in diethylpyrocarbonate-treated H_2O to a final concentration of 10 ng/μl per subunit for two-electrode voltage-clamp recordings, 20 ng/μl for patch-clamp recordings, and 300 ng/μl for immunodetection. Oocytes were injected with 32 nl of cRNA and incubated for 1–2 days at 16 °C in a low-sodium CulORS (10 mM NaCl, 80 mM *N*-methyl D-glucamine, 1 mM KCl, 2 mM $CaCl_2$, 5 mM HEPES, 2.5 mM sodium pyruvate, 0.06 mM penicillin G, and 0.02 mM streptomycin sulfate at pH 7.4). Patch-clamp recordings were performed 2–7 days after injection. To inhibit the endoprotease furin, furin inhibitor I (40 μM; Cayman Chemical, Hamburg, Germany) was added to the low-sodium CulORS.

Two-electrode voltage-clamp recordings

Recording of I_M was performed as described previously (7) using a Turbo Tec-03X amplifier (NPI, Tamm, Germany). If not stated otherwise, the V_M was clamped to −60 mV, and current signals were low-pass–filtered at 1 kHz. ENaC-mediated fractions of I_M were determined with the ENaC inhibitor amiloride (100 μM; Sigma-Aldrich, Taufkirchen, Germany) and

Table 2

Primer sequences used for site-directed mutagenesis and epitope tagging

Single nucleotide exchanges for site-directed mutagenesis are in bold type. Kozak consensus sequences are displayed in italics, and sequences coding for HA or V5 epitope tags are underlined.

Primer	Primer sequence (5′–3′)
β_{S540C}-ENaC	
Forward	ACCGCCAAGTTG**C**ACAGGAGCCAGAC
Reverse	GTCTGGCTCCTGT**G**CAACTTGGGCGGT
$\alpha_{HA/V5}$-ENaC	
Forward	ACTCTCGAG*GCCACC*ATGTACCCATACGATGTTCCAGATTACGCTGAGTCCACAGAAAAAGAGAAAAAG
Reverse	AGTTCTAGATTACGTAGAATCGAGACCGAGGAGAGGGTTAGGGATAGGCTTACCGGAAAAGGTATTTATTTCCCCATTAAA
$\delta_{HA/V5}$-ENaC	
Forward	ACTGTCGAC*GCCACC*ATGTACCCATACGATGTTCCAGATTACGCTACTAAGGAGGAGAAGAATGAG
Reverse	GAATGCGGCCGCTTACGTAGAATCGAGACCGAGGAGAGGGTTAGGGATAGGCTTACCGTTCCTTCTACCTCCATTCTCCTCATA
$\gamma_{HA/V5}$-ENaC	
Forward	ACTGTCGAC*GCCACC*ATGTACCCATACGATGTTCCAGATTACGCTTCTAAAAGTGGGAAGAAACTG
Reverse	GAATGCGGCCGCTTACGTAGAATCGAGACCGAGGAGAGGGTTAGGGATAGGCTTACCGAGTCTTTCTACATCCTCATCAGA

defined as amiloride-sensitive currents (ΔI_{ami}). Unless stated otherwise, ΔI_{ami} was consistently determined after the oocyte was perfused with ORS for 3 min. All recordings were performed at room temperature.

Patch-clamp recordings

Patch-clamp recordings were performed in the cell-attached configuration using mechanically devitellinized oocytes. Patch-pipettes (6–9-megaohm resistance) were pulled from borosilicate glass capillaries employing a two-stage puller, PP-83 (Narishige, Tokyo, Japan), heat-polished, and filled with pipette solution (145 mM NaCl, 1.8 mM $CaCl_2$, 10 mM HEPES, 2 mM $MgCl_2$, and 5.5 mM glucose at pH 7.4). Chlorided silver wires served as recording electrodes and were either inserted into the patch pipette or connected to the bath solution (145 mM KCl, 1.8 mM $CaCl_2$, 10 mM HEPES, 2 mM $MgCl_2$, and 5.5 mM glucose at pH 7.4) using a 1 M KCl, 3% agar bridge. Current signals were amplified using an LM-PC patch-clamp amplifier (List-Medical, Darmstadt, Germany), low-pass filtered at 100 Hz (Frequency Devices, Haverhill, IL), and recorded at 2 kHz with Axon Clampex software (Axon Instruments, Foster City, CA) using an Axon 1200 interface. Single-channel analysis was performed with Clampfit version 10.7 (Axon Instruments). The amount of channels in each recording was stochastically estimated by comparing the number of visible channels with a theoretical amount derived from binomial distribution as described previously (7).

Immunodetection of epitope-tagged ENaC subunits

Oocyte expression of HA/V5-tagged ENaCs was confirmed by measuring V_M and excluding cells with a $V_M \leq 0$ mV. Using a 26-gauge needle, 20–30 oocytes were lysed in 10 μl/oocyte of lysis buffer (83 mM NaCl, 10 mM HEPES, 1 mM $MgCl_2$, and 1% Triton X-100 at pH 7.4) supplemented with protease inhibitors (Complete mini EDTA-free protease inhibitor mixture tablets, Roche Applied Science). Lysates were centrifuged (1500 × *g*, 10 min, 4 °C), and supernatants were collected, avoiding transfer of the lipid-enriched layer. Lysates were mixed with SDS protein-loading buffer (Roti-Load 1, Roth, Karlsruhe, Germany), boiled for 5 min at 95 °C, and loaded (25 μl) on 4–20% SDS-polyacrylamide gels. Some protein samples were treated with PNGase F (New England Biolabs, Frankfurt am Main, Germany) according to the manufacturer's instructions. Following separation in a tank blot system (Mini-Protean Tetra Cell, Bio-Rad, Munich, Germany), proteins were transferred onto polyvinylidene difluoride membranes. Membranes were blocked for 60 min in TBST (150 mM NaCl, 15 mM Tris-HCl, 4.6 mM Tris-base, and 1% Tween 20, pH 7.6) containing 5% skim milk at room temperature. Membranes were incubated with mouse IgG anti-HA (1:10,000; Thermo Fisher Scientific) or anti-V5 (1:5000; BioLegend, San Diego, CA) antibodies at 4 °C overnight. After washing with TBST, membranes were incubated with a peroxidase-conjugated rabbit anti-mouse IgG antibody (1:5000; Thermo Fisher Scientific) in blocking buffer for 1 h at room temperature. After washing the membranes in TBST, detection of target proteins was performed using enhanced chemiluminescence solution and photoreactive films (Amersham Biosciences Hyperfilm ECL, GE Healthcare, Freiburg, Germany). Band intensities were quantified using ImageJ (National Institutes of Health, Bethesda, MD) as described previously (15).

Detection of ENaC cleavage fragments at the cell surface

Before biotinylation, ΔI_{ami} was measured, and oocytes were placed back into low-sodium ORS. All biotinylation procedures were conducted on ice. Oocytes (20–30 cells/experimental group) were washed in buffer A (90 mM NaCl, 5 mM triethanolamine, 3 mM KCl, 1 mM $CaCl_2$, pH 8.0) before incubation in buffer A containing 1 mg/ml biotin (EZ-Link Sulfo-NHS-SS-Biotin, Thermo Fisher Scientific) for 20 min with gentle agitation. Biotinylation was quenched by incubating the cells in buffer A supplemented with 50 mM glycine for 10 min. Using a 26-gauge needle, oocytes were lysed in 1 ml of lysis buffer (90 mM NaCl, 20 mM Tris, and 1% Triton X-100, pH 7.4) containing protease inhibitors (Roche Applied Science). Lysates were vortexed (20 s) and incubated for 20 min on ice. After centrifugation (8000 × *g*, 10 min, 4 °C), the aqueous phase of the supernatants was collected, avoiding transfer of the lipid-enriched layer. Immobilized neutravidin-agarose beads (100 μl; Pierce) were washed with 500 μl of lysis buffer and centrifuged (1500 × *g*, 3 min, 4 °C). Protein samples were added to the beads and incubated with gentle agitation at 4 °C overnight. Samples were centrifuged (1500 × *g*, 10 min, 4 °C), and the supernatants (cytosolic fraction) were collected. The beads were washed three times with 500 μl of lysis buffer (1500 × *g*, 3 min, 4 °C) and three times with 500 μl of lysis buffer supplemented with 300

mM NaCl (1500 × *g*, 3 min, 4 °C). Beads were transferred into 100 μl of 2× SDS protein-loading buffer (Roti-Load 1, Roth), boiled at 95 °C for 5 min, and loaded (25 μl) on 4–20% gradient SDS gels. Immunoblots were performed as described above. Proper fractionation of cytosolic and membrane proteins was confirmed by reprobing membranes with rabbit polyclonal anti-pan-actin antibody (1:1000; Cytoskeleton, Denver, CO) in TBST at 4 °C overnight and a peroxidase-conjugated goat anti-rabbit IgG antibody (1:3000; Cell Signaling, Danvers, MA) in blocking buffer for 1 h at room temperature.

Data evaluation

Data are presented in scatter plots with *lines* and *error bars* representing mean ± S.E. Oocytes for each experiment were derived from at least three different donors, and the number of individual experiments is noted in *parentheses*. Immunoblots are representative of at least three independent experiments. Statistical analyses were performed using GraphPad Prism version 7 (GraphPad Software Inc., La Jolla, CA). Gaussian distribution of individual data was assessed with the D'Agostino and Pearson omnibus normality test. Normally distributed data were analyzed by Student's unpaired *t* test (two-tailed). A Welch's correction was additionally performed if variances were different. Data that did not follow Gaussian distribution were compared using the Mann–Whitney *U* test (two-tailed). Multiple groups were compared by one-way ANOVA followed by a post hoc Tukey's multiple-comparison test (two-tailed) for normally distributed data or a Kruskal–Wallis test followed by Dunn's multiple-comparison test (two-tailed) for data not following Gaussian distribution. A p value ≤ 0.05 was considered significant. All graphics were assembled and finalized using Inkscape.

Author contributions—L. W. and M. A. conceptualization; L. W. and K. S. V. formal analysis; L. W. validation; L. W., K. S. V., and A. P. investigation; L. W. visualization; L. W., K. S. V., and M. A. methodology; L. W. and M. A. writing-original draft; L. W., K. S. V., A. P., I. M., and M. A. writing-review and editing; I. M. and M. A. resources; M. A. supervision; M. A. funding acquisition; M. A. project administration.

Acknowledgments—We thank Sean Michael Gettings (Newcastle University) for generating ENaC cRNA and Dr. Tim Boswell for critical comments on the manuscript.

References

1. Rossier, B. C., Baker, M. E., and Studer, R. A. (2015) Epithelial sodium transport and its control by aldosterone: The story of our internal environment revisited. *Physiol. Rev.* **95,** 297–340 CrossRef Medline
2. Kleyman, T. R., Kashlan, O. B., and Hughey, R. P. (2018) Epithelial Na^+ channel regulation by extracellular and intracellular factors. *Annu. Rev. Physiol.* **80,** 263–281 CrossRef Medline
3. Fronius, M. (2013) Treatment of pulmonary edema by ENaC activators/stimulators. *Curr. Mol. Pharmacol.* **6,** 13–27 CrossRef Medline
4. Baines, D. (2013) Kinases as targets for ENaC regulation. *Curr. Mol. Pharmacol.* **6,** 50–64 CrossRef Medline
5. Chraïbi, A., and Horisberger, J. D. (2002) Na self inhibition of human epithelial Na channel: temperature dependence and effect of extracellular proteases. *J. Gen. Physiol.* **120,** 133–145 CrossRef Medline
6. Collier, D. M., Peterson, Z. J., Blokhin, I. O., Benson, C. J., and Snyder, P. M. (2012) Identification of extracellular domain residues required for epithelial Na+ channel activation by acidic pH. *J. Biol. Chem.* **287,** 40907–40914 CrossRef Medline
7. Althaus, M., Bogdan, R., Clauss, W. G., and Fronius, M. (2007) Mechanosensitivity of epithelial sodium channels (ENaCs): Laminar shear stress increases ion channel open probability. *FASEB J.* **21,** 2389–2399 CrossRef Medline
8. Canessa, C. M., Schild, L., Buell, G., Thorens, B., Gautschi, I., Horisberger, J. D., and Rossier, B. C. (1994) Amiloride-sensitive epithelial Na^+ channel is made of three homologous subunits. *Nature* **367,** 463–467 CrossRef Medline
9. Stockand, J. D., Staruschenko, A., Pochynyuk, O., Booth, R. E., and Silverthorn, D. U. (2008) Insight toward epithelial Na^+ channel mechanism revealed by the acid-sensing ion channel 1 structure. *IUBMB Life* **60,** 620–628 CrossRef Medline
10. Kleyman, T. R., Carattino, M. D., and Hughey, R. P. (2009) ENaC at the cutting edge: regulation of epithelial sodium channels by proteases. *J. Biol. Chem.* **284,** 20447–20451 CrossRef Medline
11. Waldmann, R., Champigny, G., Bassilana, F., Voilley, N., and Lazdunski, M. (1995) Molecular cloning and functional expression of a novel amiloride-sensitive Na^+ channel. *J. Biol. Chem.* **270,** 27411–27414 CrossRef Medline
12. Giraldez, T., Rojas, P., Jou, J., Flores, C., and Alvarez de la Rosa, D. (2012) The epithelial sodium channel δ-subunit: new notes for an old song. *Am. J. Physiol. Renal. Physiol.* **303,** F328–F338 CrossRef Medline
13. Schönberger, M., Althaus, M., Fronius, M., Clauss, W., and Trauner, D. (2014) Controlling epithelial sodium channels with light using photoswitchable amilorides. *Nat. Chem.* **6,** 712–719 CrossRef Medline
14. Babini, E., Geisler, H.-S., Siba, M., and Gründer, S. (2003) A new subunit of the epithelial Na^+ channel identifies regions involved in Na+ self-inhibition. *J. Biol. Chem.* **278,** 28418–28426 CrossRef Medline
15. Gassmann, M., Grenacher, B., Rohde, B., and Vogel, J. (2009) Quantifying Western blots: pitfalls of densitometry. *Electrophoresis* **30,** 1845–1855 CrossRef Medline
16. Snyder, P. M., Bucher, D. B., and Olson, D. R. (2000) Gating induces a conformational change in the outer vestibule of ENaC. *J. Gen. Physiol.* **116,** 781–790 CrossRef Medline
17. Hughey, R. P., Bruns, J. B., Kinlough, C. L., Harkleroad, K. L., Tong, Q., Carattino, M. D., Johnson, J. P., Stockand, J. D., and Kleyman, T. R. (2004) Epithelial sodium channels are activated by furin-dependent proteolysis. *J. Biol. Chem.* **279,** 18111–18114 CrossRef Medline
18. Thomas, G. (2002) Furin at the cutting edge: from protein traffic to embryogenesis and disease. *Nat. Rev. Mol. Cell Biol.* **3,** 753–766 CrossRef Medline
19. Haerteis, S., Krueger, B., Korbmacher, C., and Rauh, R. (2009) The δ-subunit of the epithelial sodium channel (ENaC) enhances channel activity and alters proteolytic ENaC activation. *J. Biol. Chem.* **284,** 29024–29040 CrossRef Medline
20. Carattino, M. D., Hughey, R. P., and Kleyman, T. R. (2008) Proteolytic processing of the epithelial sodium channel γ subunit has a dominant role in channel activation. *J. Biol. Chem.* **283,** 25290–25295 CrossRef Medline
21. Bruns, J. B., Carattino, M. D., Sheng, S., Maarouf, A. B., Weisz, O. A., Pilewski, J. M., Hughey, R. P., and Kleyman, T. R. (2007) Epithelial Na^+ channels are fully activated by furin- and prostasin-dependent release of an inhibitory peptide from the γ-subunit. *J. Biol. Chem.* **282,** 6153–6160 CrossRef Medline
22. Ji, H.-L., Su, X.-F., Kedar, S., Li, J., Barbry, P., Smith, P. R., Matalon, S., and Benos, D. J. (2006) δ-Subunit confers novel biophysical features to αβγ-human epithelial sodium channel (ENaC) via a physical interaction. *J. Biol. Chem.* **281,** 8233–8241 CrossRef Medline
23. Bengrine, A., Li, J., Hamm, L. L., and Awayda, M. S. (2007) Indirect activation of the epithelial Na^+ channel by trypsin. *J. Biol. Chem.* **282,** 26884–26896 CrossRef Medline
24. Diakov, A., Bera, K., Mokrushina, M., Krueger, B., and Korbmacher, C. (2008) Cleavage in the γ-subunit of the epithelial sodium channel (ENaC)

plays an important role in the proteolytic activation of near-silent channels. *J. Physiol.* **586,** 4587–4608 CrossRef Medline

25. Tavernarakis, N., and Driscoll, M. (1997) Molecular modeling of mechanotransduction in the nematode *Caenorhabditis elegans*. *Annu. Rev. Physiol.* **59,** 659–689 CrossRef Medline
26. Sheng, S., Carattino, M. D., Bruns, J. B., Hughey, R. P., and Kleyman, T. R. (2006) Furin cleavage activates the epithelial Na^+ channel by relieving Na^+ self-inhibition. *Am. J. Physiol. Renal Physiol.* **290,** F1488–F1496 CrossRef Medline
27. Hughey, R. P., Mueller, G. M., Bruns, J. B., Kinlough, C. L., Poland, P. A., Harkleroad, K. L., Carattino, M. D., and Kleyman, T. R. (2003) Maturation of the epithelial Na^+ channel involves proteolytic processing of the α- and γ-subunits. *J. Biol. Chem.* **278,** 37073–37082 CrossRef Medline
28. Carattino, M. D., Sheng, S., Bruns, J. B., Pilewski, J. M., Hughey, R. P., and Kleyman, T. R. (2006) The epithelial Na^+ channel is inhibited by a peptide derived from proteolytic processing of its α subunit. *J. Biol. Chem.* **281,** 18901–18907 CrossRef Medline
29. Thibodeau, P. H., and Butterworth, M. B. (2013) Proteases, cystic fibrosis and the epithelial sodium channel (ENaC). *Cell Tissue Res.* **351,** 309–323 CrossRef Medline
30. Marello, K., LaRovere, J., and Sommerville, J. (1992) Binding of *Xenopus* oocyte masking proteins to mRNA sequences. *Nucleic Acids Res.* **20,** 5593–5600 CrossRef Medline
31. Iijima, R., Yamaguchi, S., Homma, K., and Natori, S. (1999) Stage-specific inhibition of *Xenopus* embryogenesis by aprotinin, a serine protease inhibitor. *J. Biochem.* **126,** 912–916 CrossRef Medline
32. Uchiyama, M., Maejima, S., Yoshie, S., Kubo, Y., Konno, N., and Joss, J. M. P. (2012) The epithelial sodium channel in the Australian lungfish, *Neoceratodus forsteri* (Osteichthyes: Dipnoi). *Proc. Biol. Sci.* **279,** 4795–4802 CrossRef Medline